THE JOURNAL OF PHYSICAL CHEMISTRY B

Article

pubs.acs.org/JPCB

Dynamics of the Gel to Fluid Phase Transformation in Unilamellar DPPC Vesicles

Sureshbabu Nagarajan, Erin E. Schuler, Kevin Ma, James T. Kindt, and R. Brian Dyer*

Department of Chemistry and the Cherry L. Emerson Center for Scientific Computation, Emory University, Atlanta, Georgia, 30322, United States

ABSTRACT: The dynamics of the gel to fluid phase transformation in 100 nm large unilamellar vesicles (LUV) of 1,2-dipalmitoyl(d62)-*sn*-glycero-3-phosphocholine (d62-DPPC), has been studied by laser-induced temperature-jump initiation coupled with time-resolved infrared spectroscopy and by MD simulations. The infrared transients that characterize the temperature dependent phase transformation are complex, extending from the nanosecond to the millisecond time scales. An initial fast (submicrosecond) component can be modeled by partial melting of the gel domains, initiated at pre-existing defects at the edges of the faceted structure of the gel phase. Molecular dynamics simulations support the model of fast melting from edge defects. The extent of melting during the fast phase is limited by the area expansion on melting, which leads to a surface pressure that raises the effective melting temperature. Subsequent melting is observed to follow highly stretched exponential kinetics, consistent with collective relaxation of the surface pressure through a hierarchy of surface undulations with different relaxation times. The slowest step is water diffusion through the bilayer to allow the vesicle volume to grow along with its expanded surface area. The results demonstrate that the dominant relaxation in the gel to fluid phase transformation in response to a large *T*-jump perturbation (compared to the transition width) is fast (submicrosecond), which has important practical and fundamental consequences.

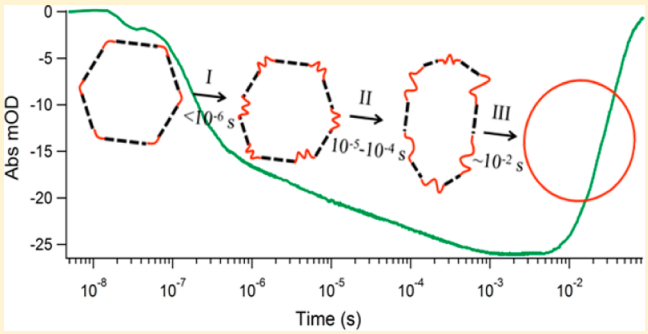

INTRODUCTION

Lipid dynamics play a critical role in a wide range of cell membrane phenomena. An important example is the dynamic formation of nanoscale liquid ordered assemblies in the cell membrane, which have been postulated to organize components to achieve specific functionality, including simple mechanical functions, signal transduction, ion transport, and membrane trafficking.[1−6] These processes may involve changes in lipid structure and dynamics and associated changes in local membrane fluidity and permeability. Understanding the dynamic organization of membranes requires elucidating the underlying structures and dynamics that span many orders of magnitude in length and time scales, from the molecular to the macroscopic. Model membrane systems have played an important role in the study of the molecular structures and dynamics that underlie macroscopic phenomena. Although the cell membrane is a mixture of hundreds of lipid types, the phase behavior of simple model phospholipid bilayers is of interest not only as a starting point for understanding the cell membrane, but also for potential applications in bionanotechnology. Here we focus on the dynamics of a phase transition in a simple model unilamellar vesicle that may serve as a basis for elucidating the dynamics of more complex phenomena in the lipid bilayer.

The phospholipid 1,2-dipalmitoyl-*sn*-glycero-3-phosphocholine (DPPC) forms stable, well-characterized unilamellar lipid vesicles. The equilibrium phase behavior of DPPC bilayers has been extensively studied. The equilibrium phase behavior of unilamellar DPPC bilayers exhibits four distinct phases, the crystal ($L_{c'}$), gel ($L_{\beta'}$), ripple ($P_{\beta'}$), and fluid or liquid-crystalline (L_α) phases in order of increasing temperature. The sharpest and most endothermic transition (ΔH = 33 kJ/mol) is the "main transition" between the highly ordered gel phase and the disordered fluid phase. Notably, the main transition (T_m = 41 °C, conveniently near normal human body temperature) produces a sharp increase in permeability that is the basis for the use of DPPC liposomes to deliver anticancer drugs selectively to solid tumors subjected to hyperthermia therapy.[7,8] The underlying molecular changes in this main transition include the conversion of lipid acyl chains from the nearly all-trans configuration to one having an increased number of gauche "kinks," and associated increases in the interfacial area per lipid and in the lipid conformational disorder and mobility.[4] The $L_{\beta'}$ to $P_{\beta'}$ transition has been observed in large unilamellar vesicles (LUV),[9] although it is not clear how the 10−15 nm periodicity of the ripple phase is influenced by the 50 nm radius of curvature.[10] All of these phase changes influence the membrane structure and dynamics. In the past several decades, the focus of studies of membrane phase behavior has been on understanding the thermodynamics and structures of the gel

Received: October 4, 2012
Revised: November 5, 2012
Published: November 6, 2012

and fluid ordered and disordered phases and the transitions between them. The dynamics of the gel to fluid phase transition is less well understood, however, due to the lack of structural specificity of the time-resolved methods used to observe the nanosecond to millisecond events.[11−15] Relaxation methods have been the primary tool used to explore the dynamics of phase transitions, probed by light scattering,[16,17] calorimetry,[18,19] ultrasound,[20] and dielectric relaxation.[20] A hierarchy of relaxation times is observed due to the complexity of the physical changes involved in phase transitions. These methods do not directly determine the molecular origin of the observed relaxation times, so the results are generally interpreted using physical models and in light of more structurally specific measurements of the dynamics. The fastest relaxation modes have been assigned to the correlation times of lipid head groups (10^{-11}−10^{-10} s), to chain segmental motions (10^{-9} s), to lateral diffusion of lipid monomers (10^{-8} s), and to gauche−trans isomerization (10^{-6} s) by analogy to NMR measurements of specifically deuterium labeled lipids.[21] Slower relaxation processes (10^{-6}−10^{-2} s) have been assigned to domain fluctuations, based on statistical mechanical models that predict a critical slowing of the lifetime near the transition temperature.[19,20] More recently, efforts have focused on developing molecular models of the dynamics of lipid phase transitions using molecular dynamics simulations.[22−25] Experimental evidence is still needed to complement these efforts and to test the validity of the computational models. Insight about how well the force fields predict the observed lipid dynamics is useful for evaluating simulations of more complex phenomena such as the formation of cholesterol-containing liquid ordered phases.

In this work, we have used an integrated experimental and theoretical approach to investigate the lipid dynamics during the gel to fluid phase transition and subsequent relaxation of the vesicle structure in 100 nm homogeneous perdeuterated d62-DPPC unilamellar vesicles. We have applied a new experimental approach to this problem consisting of laser temperature jump (*T*-jump) initiation coupled with time-resolved infrared spectroscopy to follow the molecular details of the phase transition from nanoseconds to milliseconds. *T*-jump methods allow the exploration of the dynamics far from equilibrium, particularly for a *T*-jump that is large compared to the width of the phase transition. Previous studies have used laser *T*-jump coupled with X-ray methods to study the structural transitions of lipid bilayers in water, but did not resolve the dynamics.[26,27] IR spectroscopy is a powerful, nonperturbing technique that is sensitive to acyl chain conformation, headgroup environment, and water interactions. Time-resolved IR spectroscopy can follow these structures on time scales ranging from the ultrafast conformational dynamics of the monomer to the slower global relaxation of a lipid bilayer and associated processes such as water permeation.[28] Therefore, it is possible to connect the molecular dynamics with the macroscopic phenomena using this approach. Deuterated DPPC was chosen, since the CD_2 symmetric stretch falls in a clear region of the FTIR spectrum and hence is useful to probe membrane properties in the presence of other components, including peptides and other (nondeuterated) lipids. The infrared transients that characterize the gel to fluid phase transition of DPPC are complex, extending from the nanosecond to the millisecond time scales. The dominant phase is fast (submicrosecond) and is well modeled as a partial melting of the gel domains, initiated at pre-existing defects at the edges of the faceted structure of the gel phase. Molecular dynamics simulations of a buckled lipid bilayer support the model of rapid melting proceeding from the partially disordered edge structure.

MATERIALS AND METHODS

Sample Preparation. The d62-DPPC lipids and extrusion kit were purchase from Avanti Polar Lipids, Inc. A 360 μL portion of a 25 mg/mL solution of d62-DPPC in chloroform was pipetted into a 2 mL glass vial and dried by N_2 gas, after which the sample was placed under vacuum for at least 5 h to ensure complete removal of solvent. The dried lipid film was hydrated with 300 μL of 20 mM sodium phosphate buffer at pH 7.4 with 150 mM NaCl for at least 30 min followed by at least five freeze thaw cycles starting at a temperature above the T_m and then quenching to 4 °C on ice. Unilamellar vesicles of 100 nm were prepared by extruding the hydrated solution 15 times or more through a polycarbonate filter having pore openings of 100 nm diameter, at a temperature 10 − 20 °C above the T_m of the vesicles. Transmission electron micrographs of the vesicles indicate that they are within the expected size range. For the equilibrium and temperature jump experiments, the samples were used immediately after the extrusion procedure.

FTIR Spectroscopy. Equilibrium FTIR temperature-dependent spectra were recorded on a Varian 3100 FTIR spectrometer equipped with liquid nitrogen cooled mercury cadmium telluride (MCT) detector. The spectra were the result of 256 scans recorded at a resolution of 2 cm^{-1}. The d62-DPPC lipid vesicles were prepared as described above in buffer containing 20 mM sodium phosphate and 150 mM sodium chloride at a pH* of 7.4, in D_2O [pH* refers to the uncorrected (for D_2O) pH-meter reading at 25 °C]. The d62-DPPC lipid concentration for IR experiments is approximately 30 mM. A split IR cell composed of CaF_2 windows was utilized with a path length of 100 μm to record the spectrum of both the reference (D_2O buffer solution) and the sample (d62-DPPC lipid vesicles in D_2O buffer) side of the IR transmission cell under identical conditions at each temperature. The temperature of the IR cell was controlled by a water bath, and the sample temperature was measured by a thermocouple attached to the cell. The absorbance spectra of the lipid vesicles were determined from the negative logarithm of the ratio of the single beam spectra of the sample to the reference side of the IR split cell at each temperature.

Temperature-Jump, Time-Resolved IR Measurements. The *T*-jump time-resolved IR apparatus used to measure the lipid relaxation kinetics in this study has been previously described.[29,30] The *T*-jump experiment is a pump−probe experiment in which a short pulsed (10 ns) 1.91 μm laser pulse constitutes the pump that is absorbed by the D_2O solvent and causes a rapid (10 ns) *T*-jump in the sample. The *T*-jump initiates the gel to fluid phase transformation. A quantum cascade laser (Daylight Solutions Inc., Poway, CA) tunable either in the 1565−1735 cm^{-1} or the 2035−2145 cm^{-1} region is used to probe structural changes in the sample as the system relaxes to a new equilibrium at the final temperature in response to the *T*-jump. The changes in transmission of the IR probe beam are detected by a fast (200 MHz) photovoltaic MCT detector (Kolmar Technologies, Newburyport, MA). The 1.91 μm (10 ns fwhm Gaussian pulse width, ∼30 mJ/pulse) pump radiation is obtained from a H_2 (g) filled Raman shifter (1 Stokes shift) pumped by a 10 Hz repetition rate Q-

switched DCR-4 Nd:YAG laser (Spectra Physics, Mountain View, CA) and is absorbed by weak combination bands in the D_2O solution. This pump wavelength was chosen to achieve nearly uniform heating in the pump−probe overlap region, because 87% of the pump intensity is transmitted through the 100 μm path length sample cell. The same split cell used for the equilibrium FTIR experiments was used for the kinetic measurements with the reference D_2O buffer compartment serving as an internal thermometer to determine the magnitude of the *T*-jump. The lipid relaxation transients were extracted by subtracting the change in absorbance of the reference (D_2O buffer) from the sample (d62-DPPC in D_2O buffer) in response to the *T*-jump. The kinetic traces were recorded from 10^{-9} to 10^{-2} s using a Tektronix 7912 digitizer capable of switching the time base at 5 different time points during the acquisition, to achieve uniform sampling over 7 decades in time. The data analysis was performed in IGOR Pro (Wavemetrics, Inc.).

Simulation Methods. A DPPC gel was created as previously described.[25] Thirty-two lipids arranged in the crystalline conformation were solvated by 800 waters, and first equilibrated at 273 K for 10 ns at 1 bar pressure. The structure was then replicated 8-fold along the X axis and 2-fold along the Y axis to yield a 512-lipid, 12 800-solvent box with dimensions 26.7 × 5.0 × 7.2 nm, with the tail tilt aligned with the Y axis. This structure was then subject to uniaxial compression over a 3.0 ns simulation at 310 K, with a reference pressure of 400 bar in the X direction and 1 bar in the Y and Z. The resulting structure (dimensions 21.8 × 5.1 × 8.8 nm) contained two sharp bends, but maintained nearly regular packing of its tails. This buckled structure was subject to 50 ns further MD simulation under fixed X and Y box dimensions, with pressure coupling in the Z dimension set at 1 bar pressure, at temperatures above and below the estimated transition temperature of 308 K previously determined for this force-field.[25] Simulations were performed using Gromacs 4.5[31] using the united-atom DPPC forcefield of Berger et al.[32] and a time step of 2 fs. Electrostatic forces were treated using the particle-mesh Ewald method[33] with standard Gromacs parameters. Temperature and pressure coupling were achieved using the Berendsen method.[34]

RESULTS AND DISCUSSION

Equilibrium Phase Behavior of d62-DPPC LUV. FTIR spectroscopy is ideally suited to characterize the equilibrium phase behavior of DPPC vesicles. Figure 1A shows the temperature-dependent (10 to 44 °C) FTIR spectra of LUV in D_2O buffer, in the region of the CD_2 symmetric stretching vibration of d62-DPPC. The IR absorption band for non-deuterated DPPC CH_2 symmetric stretching vibration is centered at 2850 cm^{-1}, but this mode is shifted to 2089 cm^{-1} for the deuterated lipid. The CD_2 symmetric stretch of the d62-DPPC vesicles is shifted from 2089 cm^{-1} at 10 °C to 2093 cm^{-1} at 44 °C and the bandwidth increases by ∼5−6 cm^{-1}. Both changes are consistent with the melting of the ordered gel phase to a disordered fluid or liquid crystalline phase. The shift to higher frequency is due to a loss of the mode coupling (inter- and intrachain) that is present in the tightly packed, nearly all-trans conformation (this coupling lowers the CD_2 stretching frequency), but is absent in the disordered phase due to isomerization of the acyl chain to include some gauche conformations. These gauche "kinks" disrupt intrachain mode coupling due to unfavorable geometry,

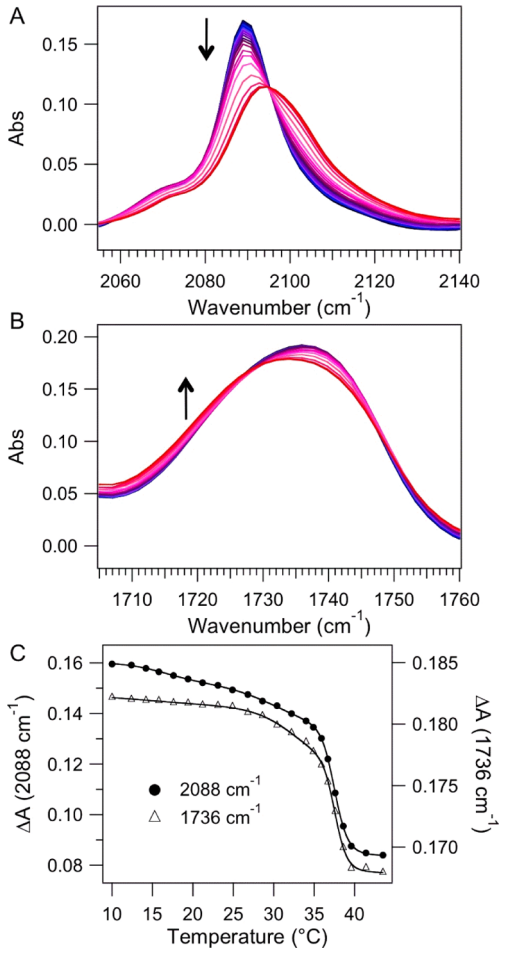

Figure 1. Temperature dependent FTIR spectra of d62-DPPC LUV in the range of 10 - 44 °C in ∼2 °C increments in (A) the CD_2 symmetric stretch and (B) the ester C═O stretch spectral regions. Arrows indicate direction of absorbance change with increasing temperature (blue = cold, red = hot). (C) Thermal phase transition of d62-DPPC obtained by plotting the intensity of the CD_2 stretch (2088 cm^{-1}) and C═O stretch (1736 cm^{-1}) versus temperature. The two curves are scaled separately for ease of comparison (note that the 1736 cm^{-1} ΔA values are significantly smaller than those at 2088 cm^{-1}). Solid lines are fits to a three sigmoid equation (eq 1).

and the concomitant increase in interchain distance disrupts interchain coupling. The increase in bandwidth is due to the increased acyl chain disorder, causing an increase in the inhomogeneous broadening. The weaker band at 2070 cm^{-1} is attributed to the symmetric stretching vibration of the terminal methyl group of the lipid acyl chains. All of these changes are completely reversible upon cooling of the solution back to the starting temperature, on the time scale of the FTIR measurement (minutes).

Figure 1B presents the temperature-dependent FTIR spectra of lipid headgroup ester carbonyl stretching (C═O) vibration. This mode occurs at 1738 cm^{-1} for the gel phase at 10 °C and is shifted to 1736 cm^{-1} in the liquid crystal phase at 44 °C. The C═O vibration band is sensitive to the local dielectric of the interface and to hydrogen bonding to water. Therefore, it is a sensitive indicator of the hydration of the membrane in the lipid headgroup region. At 44 °C, the C═O vibration is downshifted, suggesting that the headgroup is better hydrated in the fluid than in the gel phase. Figure 1C shows the melt curves derived from the temperature dependence of the

dx.doi.org/10.1021/jp309832u | J. Phys. Chem. B 2012, 116, 13749−13756

intensities of the CD_2 vibration at 2088 cm^{-1} and the C═O vibration at 1736 cm^{-1}. The solid lines are fits to a three-sigmoid function to describe the three transitions between the four distinct phases: the crystal ($L_{c'}$) to gel ($L_{\beta'}$) transition (T_{m1}), the gel ($L_{\beta'}$) to ripple ($P_{\beta'}$) transition (T_{m2}), and the ripple ($P_{\beta'}$) to fluid or liquid-crystalline (L_α) transition (T_{m3}):

$$\Delta A = \frac{A_1}{1 + e^{(T_{m1}-T)/r_1}} + \frac{A_2}{1 + e^{(T_{m2}-T)/r_2}} + \frac{A_3}{1 + e^{(T_{m3}-T)/r_3}} + b \quad (1)$$

The melt temperatures of each of these transitions determined from the fit of the CD_2 stretch data are T_{m1} = 16.4 ± 0.8 °C; T_{m2} = 30.7 ± 0.8 °C; and T_{m3} = 37.5 ± 0.1 °C, respectively. The C═O data yield the same transition temperatures within experimental error. The gel to ripple, and ripple to fluid phase transition temperatures derived from the fits are in agreement with other spectroscopic and calorimetric results (T_m = 35−37.5 °C).[35−37] The small variations in the main phase transition temperature reported for d62-DPPC by different groups may be attributed to the different accuracies of the measurements or to variability in the vesicle size (radius of curvature) and hence specific melt temperature.

Phase Transformation Dynamics. Temperature-jump initiation coupled with time-resolved infrared spectroscopy is a highly sensitive technique that allows us to directly follow the dynamics of any system that undergoes a temperature dependent structural transition within a time range of nanoseconds to hundreds of milliseconds.[38] We have used a 10 ns laser induced T-jump to initiate the main phase transformation in d62-DPPC LUV, and probed the resulting dynamics using the CD_2 symmetric stretching vibration at 2089 cm^{-1}. Figure 2A shows the time-resolved IR absorbance of d62-DPPC LUV monitored at 2089 cm^{-1} in response to a laser induced T-jump from various starting temperatures. The T-jump magnitude is 4−7 °C and the initial temperature is below T_m in all cases. A range of starting temperatures was probed to determine the temperature dependence of the relaxation rates. A transient bleach is observed at this probe frequency, as expected for the transition from an ordered gel to disordered liquid crystalline phase, based on the equilibrium FTIR data presented in Figure 1. The T-jump IR transients observed at 1712 cm^{-1}, which monitors the ester C═O stretch of the lipid headgroup, show the same general features as those observed for the CD_2 vibrations. Both are dominated by an initial response on the nanosecond time scale, followed by an extended nonexponential phase on the microsecond time scale. The 1712 cm^{-1} transients are noisier, however, due to the smaller absorbance change for this band, hindering accurate fitting of these data.

The relaxation transients exhibit complex kinetics spanning several orders of magnitude in time. The transients could not be fit to a single exponential or to a multiexponential function and hence were fit to single exponential (the dominant phase), crossing over smoothly to a stretched exponential (eq 2):

$$\Delta A(t) = c_1[\exp(-t/\tau_1) - 1],\ 0 < t < t_c$$
$$= c_2\exp(-t/\tau_2)^\alpha - c_{tot},\ t > t_c \quad (2)$$

This function resembles the "coupling model" function used to describe relaxation in glass-forming systems[39] in its inclusion of a crossover time t_c between single-exponential and stretched-exponential regimes, but differs in specifics. The time constants of the initial single-exponential component and the stretched exponential are represented by τ_1 and τ_2, the stretch factor by α, the onset time of the stretched exponential regime by t_c, and the total amplitude of the transient change in absorbance by c_{tot}. From these five independently variable fitting parameters, the amplitude prefactors of the single and stretched exponential stages (c_1 and c_2) are obtained from the constraints of continuity in the function and its first derivative at t_c (see Appendix A for details). Optimal fit values are given in Table 1. The transient corresponding to the lowest temperature T-jump, from 27.4 to 34 °C, is equally well fit by a simple stretched exponential function. This T-jump is completely within the gel ($L_{\beta'}$) to ripple ($P_{\beta'}$) phase transition. All of the other T-jumps reported here extend into the fluid phase. The distinct single exponential regime is apparently characteristic of the main transition.

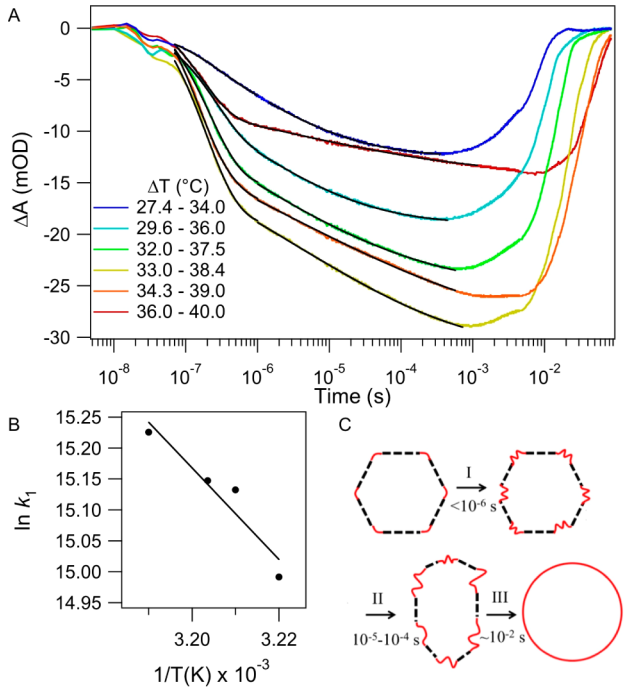

Figure 2. LUV dynamics following a laser induced T-jump. (A) Relaxation kinetics of d62-DPPC LUV monitored at 2089 cm^{-1} (CD_2 symmetric stretch) in response to a T-jump of magnitude of 4−7 °C. The legend indicates the initial and final temperatures for each jump. The kinetic traces are the average of 2500 laser shots. The solid lines are fits to eq 2. (B) Arrhenius plot of the initial rate for jumps to the fluid phase. (C) Cartoon of stages in vesicle melting. Dashed lines represent gel phase domains, red curves represent fluid phase regions.

The transients for T-jumps within the main transition are best fit by eq 2. Significant portions of the transient absorbance change are completed both before and after the crossover time, which lies near 1 μs. A number of interpretations are possible for the initial rapid response and subsequent slowing-down of the change in acyl chain CD_2 IR absorbance. The initial single-exponential component of the response could be attributed to changes in tail packing within the phases, while the slow component corresponds to melting of gel phase into fluid. This interpretation is not consistent with the observed equilibrium temperature dependent FTIR data, however, which show absorbance changes of at most −1.3 mOD per degree below the main transition onset. The predicted change is not great

dx.doi.org/10.1021/jp309832u | J. Phys. Chem. B 2012, 116, 13749−13756

Table 1. *T*-Jump IR (2089 cm^{-1}) Relaxation Parameters from Fits to Eq 2

T-jump (°C)	τ_1 (ns)	τ_2 (ns)	α	t_c (ns)	c_1 (mOD)	c_2 (mOD)	c_{tot} (mOD)	$-d\mathrm{Abs}_{2089}/dt$ (mOD/ns)	$-dA_{gel}/dt$ (nm^2/ns)	$-dA_{gel}/dt$ (predicted)
27−34	256	318	0.234	450	6	22	12	0.024	60	43
29−36	310	426	0.236	910	12	23	19	0.040	67	41
32−37	308	5142	0.297	1129	16	15	23	0.052	42	35
33−38	268	1127	0.312	1061	20	16	29	0.073	43	35
34−39	264	1027	0.259	1043	17	16	26	0.066	36	30
36−40	244	603	0.129	1002	10	14	14	0.040	24	26

enough to account for the observed magnitude of the initial fast response.

A more likely origin of the fast initial kinetic transient is the physical conversion of gel phase to fluid phase DPPC. Assuming the fast initial changes in IR absorbance reflect conversion of gel or ripple phase DPPC to fluid phase DPPC, we can estimate the initial rate of melting ($-dA_{gel}/dt$) from the initial rate in change of the signal ($d\mathrm{Abs}_{2089}/dt$, Table 1) and the total change in equilibrium absorbance over the phase transition ($\Delta\mathrm{Abs}_{2089,total}$) determined from the melt curve:

$$-dA_{gel}/dt = (A_{total}/\Delta\mathrm{Abs}_{2089,total})d\mathrm{Abs}_{2089}/dt \quad (3)$$

The total gel vesicle area, A_{total} is assumed to equal 2.5×10^4 nm^2 based on the 100 nm average diameter of the LUV. The initial rate values ($-dA_{gel}/dt$) calculated for each *T*-jump are summarized in Table 1.

Schrader et al. have recently identified a relaxation process with a time constant "τ_0" of ∼100 ns in the ultrasonic spectra of DMPC vesicles near their T_m, (within 2°) tentatively assigned to "local shape deformations of the vesicles".[20] We propose that the fast melting phase observed in the IR *T*-jump experiments is a nonequilibrium manifestation of this mode, and provides insight into its nature. The shift in the CD_2 IR absorption feature at this time scale indicates that this mode arises from the transition of lipid tails between ordered and disordered environments, and that (when driven by a large enough perturbation) the mode amplitude can encompass the phase change of a substantial fraction of the lipids in the vesicle. Under equilibrium conditions, the mode could be associated with smaller-amplitude excursions of the ordered/disordered domain boundaries, coupled to local shape deformations. In ultrasonic spectra, the mode is not observed at temperatures lower than $T_m - 2$ K, which could either indicate that the structure associated with this mode is absent at low *T* or that the mode amplitude is very weak. In the current experiments, the submicrosecond response appears unambiguously and without a lag period in *T*-jump profiles starting from temperatures as low as 7° below T_m, suggesting that the structure from which the mode develops is already present.

The conventional kinetic mechanism for a melting transition involves first the slow, activated nucleation of domains of the fluid phase, followed by a more rapid size increase of new domains, and finally a slow annealing phase as defects between domains are resolved through large-scale realignments. The fast response can be reconciled with this model if the barrier to nucleation of the new phase is negligible, which would require the presence of defects that can act as nucleation sites. Since faceting has been observed for vesicles of diameter 50−200 nm using cryo-electron microscopy,[40,41] defects at the ridges joining facets are likely an intrinsic feature of the gel-phase LUV structure. We hypothesize that curvature stress and packing defects at these ridges produce an effective local transition temperature lower than the bulk T_m, or in other words that the lipids at these defects are in a fluid state at equilibrium even below T_m. These premelted ridges are candidates for nucleation sites for fast melting of the individual facets. Evidence to support premelting at ridges, which has been proposed previously to explain temperature-dependent permeability trends in LUVs,[7] comes from atomistic molecular dynamics simulations of ridge-like structures. Uniaxial compression of a gel-phase bilayer sheet was used to prepare a buckled gel-phase structure with localized regions of high curvature. The effect of temperature on this structure is shown in Figure 3.

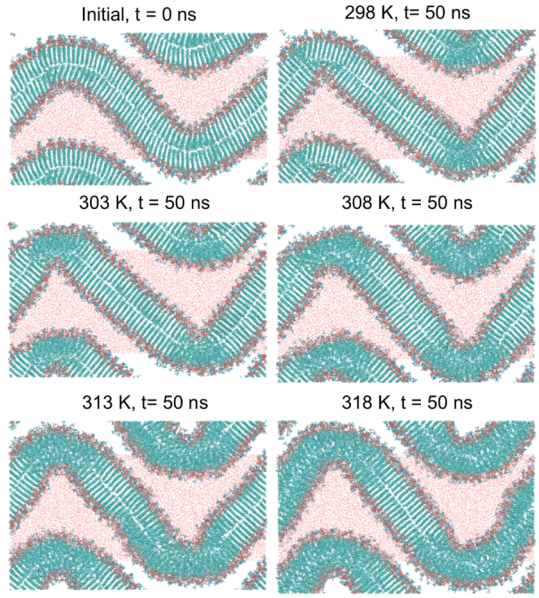

Figure 3. Snapshots from molecular dynamics simulations of buckled gel-phase DPPC bilayer. Partial replicas of the lipid component are shown to indicate continuity of the bilayer across periodic boundaries; solvent is shown (red dots) in primary box only.

At 308 K (the estimated T_m for DPPC using this force field[25]), the orderly packing of the gel phase, evident from the nearly straight and evenly spaced tails, is disrupted in the zones of high curvature. At 303 K, disordering at the bends is also apparent in more narrow zones, while at 298 K one bend is disordered while the other retains regular packing on the outer leaflet. At 313 K, melting has extended from the bend into one leaflet of the flat portion of the bilayer, and at 318 K one of the two flat sections of bilayer is entirely melted. The simulation results therefore confirm that lipids at ridge sites may be disordered in an otherwise ordered bilayer below T_m. Furthermore, the results suggest that the extent of premelting depends on *T* and that above T_m melting proceeds rapidly from

dx.doi.org/10.1021/jp309832u | J. Phys. Chem. B 2012, 116, 13749−13756

the ordered/disordered boundary. Ordered/disordered boundaries have also been described as equilibrium features of molecular models of the ripple phase[42] and may play a role similar to that of ridge defects as nucleation sites for melting.

As an additional test of the hypothesis that the submicrosecond change in IR spectrum reflects rapid initial melting from defects, we compare the observed rates to predictions based on estimates for the lengths of the boundary edges and the rate of transition from gel to fluid. For instance, a regular icosahedron of area equal to that of a 100 nm diameter vesicle would have a total ridge length of 1.6 μm; assuming that melting proceeds in both directions from each ridge gives a total interfacial front length of 3.2 μm. The postnucleation rate of the melting transition in DPPC has been estimated experimentally in terms of the velocity of advancement of a gel/fluid interface of 2×10^{-3} m K^{-1} $s^{-1} \times (T - T_m)$.[10] In the vesicles at equilibrium at the starting temperature of the T-jump, the boundary between the premelted ridge region and the ordered region will be localized wherever the effective T_m determined by local curvature equals the actual temperature. Substituting the lower temperature as the effective local T_m, the initial rate of melting after the T-jump is therefore 2×10^{-3} m K^{-1} $s^{-1} \times \Delta T$. Multiplying the estimate of 3.2 μm for the total front length by this rate produces initial rates of the same order as those seen in experiment (final column of Table 1). Therefore, we conclude that the initial fast response can be plausibly attributed to melting nucleated at ridge defects. Additional evidence that supports this interpretation comes from an Arrhenius analysis of the fast exponential phase, shown in Figure 2B. The activation energy derived from this analysis is 62 kJ/mol, about double the reported enthalpy of melting for DPPC vesicles (29−30 kJ/mol),[9] and in good agreement with a previous estimate from simulations of the apparent activation energy for retraction of the gel phase edges of 68 kJ/mol.[25]

After one microsecond, the initial exponential melting phase smoothly converts to a highly stretched exponential melting phase that spans several orders of magnitude in time. To explain the tremendous slowing-down of the melting process, we consider the approximately 24% area expansion involved in the gel-fluid transition. As area expands, the resulting surface pressure (negative surface tension) will raise the effective melting temperature and slow the melting process.[43] This surface pressure may result in wrinkling of the newly formed fluid phase, shown in step I of Figure 2C. Without any mechanism for its relaxation, accumulation of surface pressure is expected to produce a simple exponential decrease in the gel fraction, with melting asymptotically slowing down as the effective melting temperature approaches the actual temperature (see Appendix B). However, the vesicle in its partially melted state will tend to distort to dissipate this surface pressure and associated curvature stresses, a process that likely involves a hierarchy of undulatory modes with different relaxation times, including collective shape changes to the entire vesicle (Figure 2C, step II). In glass-forming systems, crossover from single- to stretched-exponential relaxation dynamics is attributed to a transition from localized to collective relaxation modes; in the present system, the onset of the stretched exponential dynamics seen in the IR transients can be attributed to a transition from independent melting of individual domains to melting that is limited by the rate of surface stress relaxation through cooperative reorganization.

The final stage in relaxation requires solvent transport through the membrane to enable the vesicle to expand its internal volume to reach a minimized curvature stress at its new, higher surface area (Figure 2C, step III). The typical time scale for volume relaxation following changes in osmotic pressure in fluid-phase LUVs is of the order 10^{-2}−10^{-1} s.[44] Our experiments provide indirect evidence that water transport through the membrane driven by the expanding vesicle occurs on the hundreds of microseconds to milliseconds time scale. The water diffusion process may not be complete within the observation time of the T-jump, however, because the transient absorbance never reaches the expected equilibrium value from the FTIR measurements. The maximum ΔA reached (before the solution begins to cool), expressed as a percentage of the equilibrium value is 100, 79, 71, 62, and 36% for jumps to 36, 37.5, 38.4, 39, and 40 °C, respectively. Clearly, a significant fraction of the amplitude is not captured for jumps to a final temperature that is above T_m. The further the jump into the fluid phase, the longer the relaxation time due to both the slow collective relaxation and water diffusion processes and therefore less of the expected change occurs within the fixed time window of the T-jump.

At still longer times, the small volume of solution (roughly 10 nL) heated by the laser begins to cool back to the initial temperature with a lifetime of 12 ms, causing the vesicles to return to the gel phase. The cooling time is nearly constant over the temperature range probed, based on the behavior of the buffer reference solution. In contrast, the apparent cooling time of the vesicle solutions becomes progressively longer as the T-jump reaches higher temperatures, as shown in Figure 2A. Therefore, we conclude that the recovery kinetics of the gel phase are slow compared to the cooling time, and they become slower as the final temperature is increased. For jumps to a final temperature below T_m, which are less than halfway through the transition, the 100 ms repetition time of the experiment is sufficient for complete recovery of the initial gel phase (the transient signals in Figure 2A recover back to the baseline). At temperatures above 40 °C, however, the recovery becomes slow enough that the transient signal becomes progressively smaller and eventually disappears entirely due to the buildup of a steady-state population of the fluid state. Slowing the laser repetition rate from 10 to 1 Hz allows the sample to recover sufficiently between laser pulses so that the transient signal reappears. We are unable to quantitatively determine the kinetics of reforming the gel phase because they are convoluted with the thermal transport kinetics occurring on nearly the same time scale. It is clear, however, that the kinetics depend strongly on the extent of melting of the vesicles. Nucleation of the gel phase from the completely melted vesicles occurs on the hundreds of milliseconds time scale, such that reforming the gel phase is only observed by drastically slowing down the repetition rate of the experiment.

■ CONCLUSIONS

We have determined the dynamics of the main gel to fluid phase transition in DPPC large unilamellar vesicles. Although the dynamics of the phase transformation is complex, the dominant phase is extremely fast, with a relaxation time of a few hundred ns. A practical consequence of the fast transformation is the possibility of rapidly triggering membrane processes that depend on membrane fluidity, using a laser-induced T-jump. Therefore, it should be possible to study the dynamics of important membrane processes ranging from protein insertion, folding, aggregation, and function using this approach. Since the fundamental dynamics of the phase transition are so fast,

related phenomena that involve similar molecular mechanisms, such as the transition from a liquid-ordered to a liquid-disordered state, likely occur on a similar time scale or even faster. For example, tighter lipid packing is a characteristic of liquid-ordered domains and therefore the liquid ordered to disordered transition involves changes in lipid conformation and interfacial surface area, albeit of a smaller magnitude. Rapid transitions in local order and fluidity may play a functional role in many processes that take place within the membrane or at its interface.[6,45,46] For example, cells may control protein insertion, folding, and function by controlling membrane fluidity. A cell can modulate the membrane fluidity by changing the local membrane composition and therefore modulate trafficking or assembly of membrane bound complexes. The ability to rapidly switch membrane fluidity may act as a gating mechanism for such processes. The dynamics of lipids within the bilayer is also an important issue that influences many membrane processes. Our results provide a direct measure of important lipid dynamics during a phase transition and subsequent overall relaxation of the vesicle. The results provide the fundamental basis for understanding and predicting the dynamics of such processes.

APPENDIX A. RELATIONSHIP BETWEEN FITTING PARAMETERS IN EQ 2

Given τ_1, τ_2, α, t_c, and c_{tot}, the constraints on continuity of the function and its first derivative at $t = t_c$ constrain the c_1 and c_2 terms to the following:

$$c_1 = c_{tot}\left[\left(\frac{\tau_2}{\alpha\tau_1}\left(\frac{t_c}{\tau_2}\right)^{1-\alpha} - 1\right)\exp(-t_c/\tau_1) + 1\right]^{-1} \quad \text{(A1)}$$

$$c_2 = c_1\frac{\tau_2}{\alpha\tau_1}\left(\frac{t_c}{\tau_2}\right)^{1-\alpha}\frac{\exp(-t_c/\tau_1)}{\exp[-(t_c/\tau_2)^{\alpha}]} \quad \text{(A2)}$$

APPENDIX B: DERIVATION OF SINGLE-EXPONENTIAL FORM FOR VESICLE MELTING

Define A_{gel} as area of system in the gel phase, and assume that in the absence of surface pressure,

$$-\frac{dA_{gel}}{dt} = CL_{bnd}(T - T_m) \quad \text{(B1)}$$

where L_{bnd} is the length of the boundary between gel and fluid (treated as constant), C is a constant, and T_m is the transition temperature. The expansion associated with the melting process causes an increase in surface pressure P, which may be relaxed by some process or processes at a rate Γ:

$$\frac{dP}{dt} = -\frac{\chi_{melt}\kappa}{A_{tot}}\frac{dA_{gel}}{dt} - \Gamma(P, ...) \quad \text{(B2)}$$

where $\chi_{melt} \approx 0.24$ is the fractional area expansion associated with melting and κ is a surface compressibility modulus. (Because of the possibilities for local buckling, κ is not necessarily the same as the typical compressibility modulus, which relates surface tension to relative increase in area.) The effect of surface pressure (or negative surface tension) is an effective increase in the melting transition temperature by a factor $P\Delta A_{melt}/\Delta H_{melt}^{\circ}$, which will slow down the melting rate.[43] We can approximate a pressure-dependent melting rate by substituting T_m from eq B1 with a pressure-dependent transition temperature $T_m(P)$:

$$-\frac{dA_{gel}}{dt} = CL_{bnd}\left(T - T_m\left(1 + \frac{P\Delta A_{melt}}{\Delta H_{melt}^{\circ}}\right)\right) \quad \text{(B3)}$$

The overall dynamics of melting will then depend on the balance of pressure building up through the area increase associated with melting and the rate of pressure relaxation through changes in vesicle shape and volume, which are implicitly included in the relaxation rate Γ, which would be expected to depend on pressure but may depend on the structural state of the vesicle as well. If we can treat surface relaxation as negligible on the melting time scale, ($\Gamma = 0$) then these two equations yield an exponential decay in the gel-phase area until the surface pressure effect on T_m halts further melting:

$$-\frac{\Delta A_{gel}(t)}{A_{tot}} = \frac{\Delta H^{\circ}}{\chi_{melt}\kappa\Delta A}\left(\frac{T}{T_m(0)} - 1\right)\left(1 - \exp\left(-\frac{CL_{bnd}}{A_{tot}}\frac{\chi_{melt}\kappa\Delta A}{\Delta H^{\circ}}T_m(0)t\right)\right) \quad \text{(B4)}$$

AUTHOR INFORMATION

Corresponding Author

*Phone: (404) 727-6637; e-mail: briandyer@emory.edu.

Notes

The authors declare no competing financial interest.

ACKNOWLEDGMENTS

We thank Donny Magana for helpful discussions. This work was supported by NIH Grant GM053640 (R.B.D.) and NSF Grant CHE-0911285 (J.T.K.).

ABBREVIATIONS

d62-DPPC, 1,2-dipalmitoyl(d62)-*sn*-glycero-3-phosphocholine; FTIR, Fourier transform infrared; LUV, large unilamellar vesicle

REFERENCES

(1) Brown, D. A.; London, E. *Annu. Rev. Cell Dev. Biol.* **1998**, *14*, 111−136.
(2) Simons, K.; Ikonen, E. *Nature* **1997**, *387*, 569−572.
(3) Herreros, J.; Ng, T.; Schiavo, G. *Mol. Biol. Cell* **2001**, *12*, 2947−2960.
(4) Nagle, J. F.; Tristram-Nagle, S. *Biochim. Biophys. Acta* **2000**, *1469*, 159−195.
(5) London, E. *Biochim. Biophys. Acta* **2005**, *1746*, 203−220.
(6) Lingwood, D.; Simons, K. *Science* **2010**, *327*, 46−50.
(7) Mills, J. K.; Needham, D. *Biochim. Biophys. Acta* **2005**, *1716*, 77−96.
(8) Needham, D.; Dewhirst, M. W. *Adv. Drug Delivery Rev.* **2001**, *53*, 285−305.
(9) Mason, P. C.; Gaulin, B. D.; Epand, R. M.; Wignall, G. D.; Lin, J. S. *Phys. Rev. E* **1999**, *59*, 921−928.
(10) Kranenburg, M.; Smit, B. *J. Phys. Chem. B* **2005**, *109*, 6553−6563.
(11) Kharakoz, D. P.; Shlyapnikova, E. A. *J. Phys. Chem. B* **2000**, *104*, 10368−10378.
(12) Genz, A.; Holzwarth, J. F. *Eur. Biophys. J.* **1986**, *13*, 323−330.
(13) Laggner, P.; Kriechbaum, M. *Chem. Phys. Lipids* **1991**, *57*, 121−145.

(14) Genz, A.; Holzwarth, J. F.; Tsong, T. Y. *Biophys. J.* **1986**, *50*, 1043−1051.
(15) Caffrey, M. *Annu. Rev. Biophys. Biophys. Chem.* **1989**, *18*, 159−186.
(16) Tsong, T. Y.; Kanehisa, M. I. *Biochemistry* **1977**, *16*, 2674−2680.
(17) Blume, A.; Hillmann, M. *Eur. Biophys. J. Biophys. Lett.* **1986**, *13*, 343−353.
(18) Vanosdol, W. W.; Johnson, M. L.; Ye, Q.; Biltonen, R. L. *Biophys. J.* **1991**, *59*, 775−785.
(19) Grabitz, P.; Ivanova, V. P.; Heimburg, T. *Biophys. J.* **2002**, *82*, 299−309.
(20) Schrader, W.; Halstenberg, S.; Behrends, R.; Kaatze, U. *J. Phys. Chem. B* **2003**, *107*, 14457−14463.
(21) Smith, R. L.; Oldfield, E. *Science* **1984**, *225*, 280−288.
(22) Marrink, S. J.; Risselada, J.; Mark, A. E. *Chem. Phys. Lipids* **2005**, *135*, 223−244.
(23) Risselada, H. J.; Marrink, S. J. *Soft Matter* **2009**, *5*, 4531−4541.
(24) Leekumjorn, S.; Sum, A. K. *Biochim. Biophys. Acta* **2007**, *1768*, 354−365.
(25) Coppock, P. S.; Kindt, J. T. *J. Phys. Chem. B* **2010**, *114*, 11468−11473.
(26) Tenchov, B.; Koynova, R.; Rapp, G. *Biophys. J.* **1998**, *75*, 853−866.
(27) Rappolt, M.; Pabst, G.; Rapp, G.; Kriechbaum, M.; Amenitsch, H.; Krenn, C.; Bernstorff, S.; Laggner, P. *Eur. Biophys. J. Biophys. Lett.* **2000**, *29*, 125−133.
(28) Lewis, R. N. A. H.; McElhaney, R. N. *Methods Mol. Biol.* **2007**, *400*, 207−226.
(29) Dyer, R. B.; Gai, F.; Woodruff, W. H.; Gilmanshin, R.; Callender, R. H. *Acc. Chem. Res.* **1998**, *31*, 709−716.
(30) Williams, S.; Causgrove, T. P.; Gilmanshin, R.; Fang, K. S.; Callender, R. H.; Woodruff, W. H.; Dyer, R. B. *Biochemistry* **1996**, *35*, 691−697.
(31) Hess, B.; Kutzner, C.; van der Spoel, D.; Lindahl, E. *J. Chem. Theor. Comp.* **2008**, *4*, 435−447.
(32) Berger, O.; Edholm, O.; Jähnig, F. *Biophys. J.* **1997**, *72*, 2002−2013.
(33) Essman, U.; Perera, L.; Berkowitz, M. L.; Darden, T.; Lee, H.; Pedersen, L. G. *J. Chem. Phys.* **1995**, *103*, 8577−8592.
(34) Berendsen, H. J. C.; Postma, J. P. M.; DiNola, A.; Haak, J. R. *J. Chem. Phys.* **1984**, *81*, 3684−3690.
(35) Fraile, M. V.; Patrón-Gallardo, B.; López-Rodríguez, G.; Carmona, P. *Chem. Phys. Lipids* **1999**, *97*, 119−128.
(36) Lewis, R. N. A. H.; Pohle, W.; McElhaney, R. N. *Biophys. J.* **1996**, *70*, 2736−2746.
(37) Singh, H.; Emberley, J.; Morrow, M. R. *Eur. Biophys. J.* **2008**, *37*, 783−792.
(38) Callender, R.; Dyer, R. B. *Curr. Opin. Struct. Biol.* **2002**, *12*, 628−633.
(39) Ngai, K. L. *J. Phys.: Condens. Matter* **2000**, *12*, 6437−6451.
(40) Andersson, M.; Hamarstrom, L.; Edwards, K. *J. Phys. Chem.* **1995**, *99*, 14531−14538.
(41) Ickenstein, L. M.; Arfvidsson, M. C.; Needham, D.; Mayer, L. D.; Edwards, K. *Biochim. Biophys. Acta: Biomembr.* **2003**, *1614*, 135−138.
(42) de Vries, A. H.; Yefimov, S.; Mark, A. E.; Marrink, S. J. *Proc. Natl. Acad. Sci. U.S.A.* **2005**, *102*, 5392−5396.
(43) Uline, M. J.; Schick, M.; Szleifer, I. *Biophys. J.* **2012**, *102*, 517−522.
(44) Mathai, J. C.; Tristram-Nagle, S.; Nagle, J. F.; Zeidel, M. L. *J. Gen. Physiol.* **2008**, *131*, 69−76.
(45) Groves, J. T.; Kuriyan, J. *Nat. Struct. Mol. Biol.* **2010**, *17*, 659−665.
(46) Saxena, R.; Chattopadhyay, A. *J. Neurochem.* **2011**, *116*, 726−733.